CARBON 57 (2013) 146–160

Available at www.sciencedirect.com

ScienceDirect

journal homepage: www.elsevier.com/locate/carbon

Magnesium–carbon hydrogen storage hybrid materials produced by reactive ball milling in hydrogen

M. Lototskyy [a,*], J.M. Sibanyoni [a], R.V. Denys [b], M. Williams [a], B.G. Pollet [a], V.A. Yartys [b,c,*]

[a] HySA Systems Competence Centre, SAIAMC, Faculty of Sciences, University of the Western Cape, Private Bag X17, Bellville 7535, South Africa

[b] Institute for Energy Technology, P.O. Box 40, Kjeller NO2027, Norway

[c] Norwegian University of Science and Technology, Trondheim NO7491, Norway

ARTICLE INFO

Article history:
Received 27 September 2012
Accepted 19 January 2013
Available online 29 January 2013

ABSTRACT

Time-resolved studies uncovered kinetics and mechanism of Mg–hydrogen interactions during High energy reactive ball milling in hydrogen (HRBM) in presence of various types of carbon, including graphite (G), activated carbon (AC), multi-wall carbon nanotubes (MWCNT), expandable (EG) and thermally-expanded (TEG) graphite. Introduction of carbon significantly changes the hydrogenation behaviour, which becomes strongly dependent on the nature and amount of carbon additive. For the materials containing 1 wt.% AC or TEG, and 5 wt.% MWCNT, the hydrogenation becomes superior to that for the individual magnesium and finishes within 1 h. Analysis of the data indicates that carbon acts as a carrier of the "activated" hydrogen by a mechanism of spill-over. For Mg–G the hydrogenation starts from an incubation period and proceeds slower. An increase in the content of EG and TEG above 1 wt.% results in the deterioration of the hydrogenation kinetics. The effect of carbon additives has roots in their destruction during the HRBM to form graphene layers encapsulating the MgH_2 nanoparticles and preventing the grain growth. This results in an increase of absorption–desorption cycle stability and a decrease of the MgH_2 crystallite size in the re-hydrogenated Mg–C hybrid materials (40–125 nm) as compared to Mg alone (180 nm).

© 2013 Elsevier Ltd. This is an open access article under the CC BY-NC-ND license (http://creativecommons.org/licenses/by-nc-nd/3.0/).

1. Introduction

Magnesium dihydride MgH_2 is an attractive hydrogen storage material. It has a high reversible hydrogen storage capacity (7.6 wt.% H/~110 kg H/m^3); magnesium metal is inexpensive and abundant. At the same time, slow hydrogenation/dehydrogenation kinetics at temperatures below 350 °C and high stability (that corresponds to an equilibrium hydrogen pressure of 1.0 bar at $T \sim 300$ °C) are the major obstacles for hydrogen storage applications on the basis of MgH_2. Numerous studies have been carried out in an effort to enhance Mg hydrogenation rate [1]. One of the most promising approaches was found to be mechanical milling (MM).

MM yields nanostructured materials with improved hydrogenation–dehydrogenation kinetics because of the modification of composition and structure. In particular, it allows to produce mechanical alloy Mg–25% Fe which cannot be obtained by conventional metallurgical routes [2]. During MM a combination of a repeated cold welding and fracturing of the particles will define the ultimate structure of the powder. The product of the milling often exhibits unusual physical and chemical properties, and enhanced reactivity,

* *Corresponding authors:* Fax: +27 21 9599312 (M. Lototskyy), +47 63 81 29 05 (V.A. Yartys).
E-mail addresses: mlototskyy@uwc.ac.za, mvlot@hysasystems.org (M. Lototskyy), volodymyr.yartys@ife.no (V.A. Yartys).

http://dx.doi.org/10.1016/j.carbon.2013.01.058
0008-6223/© 2013 Elsevier Ltd.
This is an open access article under the CC BY-NC-ND license (http://creativecommons.org/licenses/by-nc-nd/3.0/).

in particular, with respect to hydrogen. The enhancements are especially pronounced for Mg-based materials where nanostructuring and surface modification result in a dramatic improvement of the hydrogenation kinetics [3]. High energy reactive ball milling in hydrogen atmosphere (HRBM) of Mg with catalytic additives has been proven to be the most efficient way to further improve the re-hydrogenation process [4,5]. Some materials, for example, containing the additive of BCC-V alloy, were characterised by exceptional performances during their re-hydrogenation, which started even at room temperature and, at optimal conditions, was completed in less than 1 min [5].

Earlier, studies of carbon-containing Mg-based hydrogen storage hybrid materials attracted special attention. Imamura et al. [6] showed that MM of Mg and graphite with organic additives (e.g. benzene, cyclohexene and cyclohexane) resulted in improvement of the hydrogenation kinetics and decrease of dehydrogenation temperature. MM (4–40 h long) resulted in generation of dangling carbon bonds in graphite, promoting the formation of C–H bonds and thus forming new hydrogen-storing sites. HRBM of graphite was shown to result in the formation of the hydrogenated carbon ($CH_{\sim 1}$; 7.4 wt.% H) where H atoms were both intercalated into the graphite interlayers, and, also formed covalent C–H bonds [7]. Similar results confirming chemisorption of H (4–6 wt.% H) in HRBM graphite were presented in [8]; the presence of iron nanoparticles introduced from milling tools resulted in an increase of the amount of the chemically bound hydrogen [9].

Huot et al. [10] has earlier demonstrated that graphite significantly accelerates reactive synthesis of MgH_2 during an hour long ball milling in H_2 (300 °C, 4.0 bar) with the formed materials showing improved hydrogenation and dehydrogenation kinetics. The use of various carbon species (graphite, activated carbon, carbon black, carbon nanotubes, fullerenes, nanodiamonds and other forms of nanoscale carbon) ball milled with Mg or MgH_2 reduces hydrogen sorption temperature, improves kinetics and also prevents MgH_2 particle growth during the hydrogenation/dehydrogenation cycling [11–22]. The observed improvements are more pronounced in case of the reactive ball milling of Mg with carbon additives in hydrogen gas [17].

It was also shown that compacting of Mg-based hydrogen storage materials with expanded natural graphite (ENG; $\geqslant$10 wt.%) results in a significant improvement of radial thermal conductivity of the obtained composites [23,24] that allowed for their industrial-scale usage in hydrogen storage systems characterized by fast dynamics of hydrogen uptake and release [24]. At the same time, the information about influence of ENG and similar materials on hydrogenation and dehydrogenation performances of HRBM Mg is still missing.

Despite intensive studies of MM and HRBM of Mg-based hydrogen storage materials, including carbon-containing ones, have been performed, information about hydrogenation behaviour of the material during HRBM is scarce. Usually, the evolution of phase–structural changes in the material during the milling is carried out by periodic sampling of the material from the milling vial followed by XRD and other analyses; less often, hydrogen absorption during HRBM is monitored directly by pressure measurements in the milling vial [25,26]. Collecting such information for HRBM of Mg-based hydrogen storage materials with various carbon additives, together with the supplementary structural, morphological and dehydrogenation/re-hydrogenation data, would be of high value to improve understanding of the mechanism governing hydrogen sorption performances and, furthermore, would promote the development of highly-efficient lightweight hydrogen storage materials.

Our earlier publications concerning studies of magnesium-based HRBM materials were mainly focused on the performance of the materials during their re-hydrogenation and phase–structural characterisation [5,27]. This paper will present in-depth data on the studies of hydrogen absorption–desorption behaviours of the synthesised by HRBM Mg–C hybrid materials containing various types of carbon, including graphite (G), activated carbon (AC), multi-wall carbon nanotubes (MWCNT), expandable (EG) and thermally-expanded (TEG) graphite, $\geqslant$1 wt.%. These materials and their hydrides were prepared and studied using synchrotron and conventional X-ray diffraction (XRD), transmission (TEM) and scanning (SEM) electron microscopy, combined differential scanning calorimetry and thermogravimetric analysis (DSC/TGA), thermal desorption spectroscopy (TDS), and by probing the kinetics of hydrogen absorption. Emphasis is on the *in situ* studies of the mechano-chemical hydrogenation of Mg in presence of various carbon additives ($\leqslant$5 wt.%). The effects of HRBM on the hydrogenation rate, thermal decomposition and re-hydrogenation performances, phase composition and microstructural evolution of Mg was studied as related to the type of carbon additives. Influence of the prehistory of the sample, thermal and surface composition, on the dehydrogenation and re-hydrogenation performances was also in the focus.

2. Experimental

The materials used in the study included commercially available powders of magnesium (250...1200 μm, 99.8%), graphite ($\leqslant$20 μm, 99+%), expandable graphite (500 μm, 99.9 + %), YP-50F activated carbon (3...20 μm), and multi-wall carbon nanotubes (diameter (5...20)·10^{-3} μm, length 10 μm, 90+%). Thermally expanded graphite was prepared by heating the expandable graphite to 900 °C in an open tube furnace, for 1 h. MgH_2 (Alfa Aesar, 98%) was used as a reference material in studies of the dehydrogenation and re-hydrogenation performances. Further details on starting materials are given in Supplementary information.

HRBM was performed in two types of planetary ball mills, Fritsch P6 and Retsch PM100, under hydrogen pressure (P_0 = 30 bar), at a rotation speed of 500 rpm. HRBM in Fritsch P6 mill was carried out using 80 ml hardened steel vial at balls-to-powder weight ratio (BPR) of 40:1 and 80:1 (sample weight 3 and 1.5 g, respectively). To monitor the hydrogenation process, the milling was periodically paused (typically in 20–30 min intervals) and the vial, after cooling to room temperature, was connected to a Sieverts-type apparatus and the pressure drop was measured; the vial was then refilled with hydrogen (30 bar), and milling was continued.

HRBM in Retsch PM100 mill was performed in a 220 ml hardened steel vial equipped with pressure–temperature monitoring system (Evico Magnetics GmbH) at BPR 40:1 (~8.0 g sample). The hydrogen pressure in the vial was kept above 20 bar by refilling the consumed hydrogen to $P \sim 30$ bar. When the vial temperature approached 70 °C, the milling was stopped and resumed again after its cooling to room temperature. The amount of hydrogen absorbed in the sample during HRBM was evaluated accounting time dependences of actual pressure–temperature values and H_2 compression factor.

The collected datasets for hydrogen absorption during HRBM and re-hydrogenation (the procedure is described below) were used in analysis of the formal kinetics of the processes performed using a modified *Avrami–Erofeev* equation:

$$\frac{C}{C_{max}} = \begin{cases} 0, & t \leqslant t_0 \\ 1 - \exp\{-[(\frac{t-t_0}{t_R})^n]\}, & t > t_0 \end{cases}; \quad (1)$$

where C, C_{max} are the actual and maximum H concentration, respectively; t is time; t_0 is the incubation period; t_R is characteristic hydrogenation time (reciprocal rate constant); and n is an exponential factor indirectly related to the reaction mechanism.

XRD studies were performed using a standard diffractometer with Cu-K_α radiation. Precise phase–structural data were collected using synchrotron XRD performed at BM01A station at Swiss-Norwegian Beamline (ESRF, Grenoble).

Morphological studies of the as-milled and re-hydrogenated materials included measurements of the particle size of the samples suspended in isopropanol, as well as high resolution SEM and TEM.

Further details on the samples preparation and their structural–morphological studies are presented in the Supplementary information, Section S1.

Hydrogen desorption from the as-milled and re-hydrogenated samples was studied by DSC/TGA. The analyses were carried out using STA 6000 analyzer (Perkin Elmer), heating from 25 to 550 °C at the heating rate of 5 °C/min. The samples ($m \sim 50$ mg) were placed, in an argon glove box, into standard alumina crucibles which were moved to the instrument in sealed containers followed by a quick installation into the sample holder. The measurements were performed under purified argon flow (100 mL/min). The heat effects of the decomposition of the studied samples were calculated by the integration of time dependences of the specific heat flow in the decomposition temperature intervals (calibration standards are specified in the Supplementary information).

DSC data was also used for the estimation of apparent activation energy of dehydrogenation by application of the Kissinger method, (heating rates of 5, 10, 15 and 20 °C/min), similar to the procedure used by Danaie et al. [28] in their study of nanocrystalline MgH_2.

Dehydrogenation and re-hydrogenation performances of the materials after HRBM were studied using a volumetric setup. 200 mg of the sample powder was loaded into the reactor which, together with the measurement system, was further evacuated to $<10^{-4}$ mbar. TDS measurements were performed by heating the reactor at a constant heating rate (5 °C/min) from 25 to 400–470 °C leading to H_2 desorption under dynamic vacuum conditions; the vacuum sensor was calibrated on the flow rate of H_2 supplied into the measurement system. Further re-hydrogenation was carried out at ~15 bar H_2 and 250 °C for ~4 h followed by cooling down to room temperature. Two TDS–re-hydrogenation cycles were performed for each sample; particular samples were studied several times, at various maximum heating temperatures in the course of TDS (further referred as "maximum temperature", 400–470 °C).

The experiments on cycle stability of HRBM Mg and Mg–5G during desorption/absorption were carried out at 350 °C; the kinetics was measured at hydrogen pressures of 10 bar (absorption) and 1 bar (desorption).

The presented data on hydrogen storage capacity of the Mg–C hybrid materials [wt.% H] were estimated based on the total weight of the sample, including both magnesium and carbon.

3. Results and discussion

3.1. HRBM behaviour

Table 1 summarizes the results on hydrogenation behaviour of magnesium and magnesium–carbon materials during HRBM using Fritsch P6 and Retsch PM100 ball mills.

Studies of hydrogenation performances of Mg and Mg–xC materials (C = G, MWCNT; x = 2, 5 and 10 wt.%) during their preparation in Fritsch P6 at BPR = 80:1 and 40:1 (see Supplementary information; Fig. S1) showed that for pure Mg, a nearly complete $Mg \rightarrow MgH_2$ transformation took place within 6 h of milling. At BPR = 80:1, graphite additives lead to the noticeable increase of the $Mg \rightarrow MgH_2$ transformation rate. However, this effect gradually weakens following the increase of the quantity of graphite in the mixture. Moreover, graphite addition leads to the appearance of the incubation period, especially pronounced at the lower BPR. Duration of the incubation period increases with increase in the quantity of graphite.

Taking into account a more profound difference in the hydrogenation behaviours for the various Mg–C materials synthesised at a lower BPR, further HRBM experiments using Retsch PM100 were carried out at BPR = 40:1.

Typical hydrogenation performances of Mg and Mg–C materials during HRBM in Retsch PM100 are presented in Fig. 1A and B and in Supplementary information (Figs. S2 and S3). Slow, but noticeable hydrogenation of Mg starts immediately and reaches completion in ~6 h of HRBM; the experimentally measured maximum hydrogen absorption capacity is very close to the theoretical value for MgH_2 (7.66%). The hydrogenation kinetics is described by typical S-shaped curves, with *Avrami* exponential factor $n \approx 4$.Introduction of carbon significantly changes the hydrogenation behaviour during the HRBM; the changes are strongly dependent on both nature and amount of carbon additive (Table 1, Fig. 1). Addition of graphite results in the appearance of a well-defined incubation period (~2 h) and does not significantly change the time required for the complete hydrogenation. However, it changes the reaction mechanism as

Table 1 – Characteristics of hydrogen storage capacities and kinetics of hydrogen absorption by magnesium and magnesium–carbon materials during the HRBM (Fig. 1).

Composite	Maximum H capacity (wt.% H)		Fitted kinetic parameters (Eq. (1))			
	Theoretical[a]	Experimental	t_0 (h)	t_R (h)	n	Pearson correlation coefficient, R^2
Mg[b] (80:1)	7.66	7.54	0	2.62(3)	3.2(2)	0.99686
Mg[b] (40:1)	7.66	7.36	0	3.47(3)	3.0(1)	0.99783
Mg	7.66	7.69	0	3.025(5)	4.27(3)	0.99706
Mg–1G	7.58	7.38	1.65(5)	1.98(1)	2.20(1)	0.99715
Mg–2G[b] (80:1)	7.51	7.48	0.23(3)	1.10(4)	2.36(9)	0.99896
Mg–2G	7.51	7.54	2.25(2)	1.12(2)	2.18(4)	0.99866
Mg–5G[b] (80:1)	7.29	7.27	0.42(3)	1.08(3)	2.11(7)	0.99905
Mg–5G[b] (40:1)	7.29	7.28	2.32(5)	1.03(6)	2.33(2)	0.99582
Mg–5G	7.29	8.10	2.23(2)	1.10(2)	1.55(4)	0.9975
Mg–10G[b] (80:1)	7.01	6.86	0.86(8)	1.72(9)	3.3(2)	0.99704
Mg–1MWCNT	7.58	7.20	0	3.58(1)	2.31(1)	0.99746
Mg–2MWCNT	7.51	7.35	0.83(1)	0.92(1)	1.27(2)	0.99549
Mg–5MWCNT[b] (40:1)	7.29	7.29	2.08(2)	0.55(3)	1.24(7)	0.99714
Mg–5MWCNT	7.29	7.37	0.31(1)	0.38(1)	1.69(4)	0.99838
Mg–1AC	7.58	7.89	0.59(1)	0.11(1)	1.43(4)	0.99066
Mg–2AC	7.51	7.87	0	2.34(1)	1.76(1)	0.99846
Mg–5AC	7.29	7.40	0.515(5)	0.88(1)	1.33(1)	0.99912
Mg–1EG	7.58	7.75	0.12(1)	3.57(1)	4.42(2)	0.99665
Mg–2EG	7.51	4.69	0	6.08(1)	2.38(1)	0.99404
Mg–5EG	7.29	0.22	Not fitted			
Mg–1TEG	7.58	7.33	0.02(3)	1.53(3)	3.6(1)	0.99872
Mg–5TEG	7.29	0.24	Not fitted			

[a] Assuming 100% formation of MgH_2 and no hydrogenation of carbon.
[b] The marked samples were studied in Fritsch P6 (BPR = 80:1 and 40:1); otherwise the HRBM experiments were carried out in Retsch PM100 (BPR = 40:1).

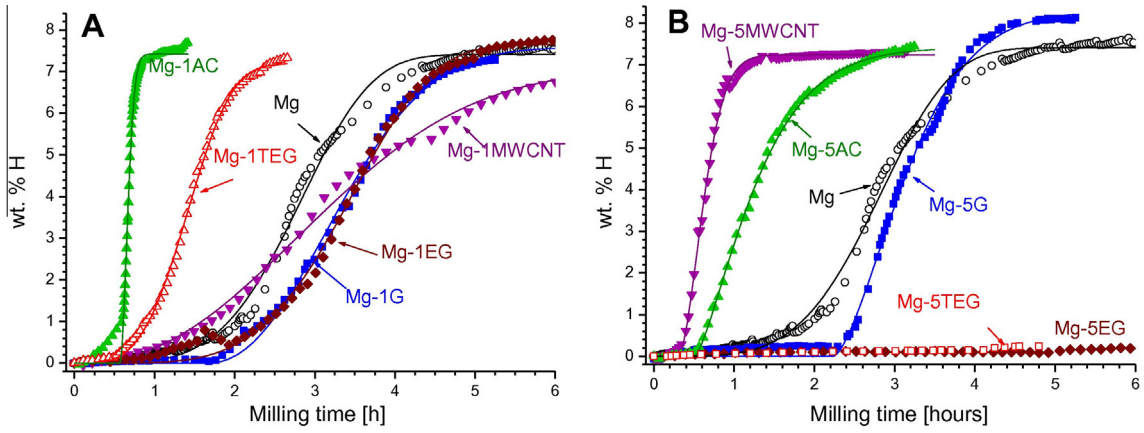

Fig. 1 – HRBM behaviour of Mg and Mg–C materials containing 1 (A) and 5 (B) wt.% of carbon additives: experimental data (symbols) and fitting results (lines).

reflected by the modification of the hydrogenation kinetics and a decrease of n to 2…1.5. Similar values of n close to 2 were also observed for a number of other Mg–C materials (Table 1).

Though the fitted parameters in kinetic equation (1) do not allow reaching an unambiguous conclusion concerning the mechanism of the hydrogenation, the n value is considered as a footprint of the process [29]. When $n \geqslant 3$ (Mg, Mg–10G, Mg–1EG, Mg–1TEG), the rate-limiting step of the reaction can only be the phase transformation, with either 3D ($n = 3$[1],4[2]) or 2D ($n = 3$[2]) growth of MgH_2 nuclei. The lower n values were observed for the other materials and indicate that the rate-limiting step changes to a phase transformation ($n = 2$ for the 2D[1] and 1D[2] growth, respectively) or to H diffusion

[1] At a constant number of nuclei.
[2] At a constant nucleation rate.

Table 2 – Crystallographic characteristics, abundances and crystallite sizes for the main constituent phases obtained from Rietveld powder refinements of the XRD data.

Sample	MgH_2 crystalline size (nm)	α-MgH_2			γ-MgH_2				Mg		
		Abundance (wt.%)	*a* (Å)	*c* (Å)	Abundance (wt.%)	*a* (Å)	*b* (Å)	*c* (Å)	Abundance (wt.%)	*a* (Å)	*c* (Å)
Mg (as milled)	6.5–7.5	69–82	4.518–4.523	3.021–3.022	18–24	4.521–4.536	5.410–5.438	4.934–4.953	0–7	3.215	5.215
Mg–1G (as milled)	7.4	94	4.523	3.027	6	4.521	5.438	4.934	0	–	–
Mg–2G (as milled)	6.2	83	4.520	3.020	15	4.521	5.438	4.934	2	3.21	5.21
Mg–5G (as milled)	6.1–6.5	76–89	4.517–4.521	3.021–3.022	11–19	4.521–4.540	5.406–5.438	4.934–4.948	0	–	–
Mg–2MWCNT (as milled)	6.5	78	4.520	3.020	17	4.521	5.438	4.934	0	–	–
Mg–5MWCNT (as milled)	5.4–6.1	74–89	4.519–4.521	3.021–3.022	10–22	4.521–4.543	5.404–5.438	4.934–4.95	0	–	–
Mg–5MWCNT (as milled; before the end of incubation period)	21	1.6	4.513	3.023	0	–	–	–	95.4 (textured)	3.205	5.204
Mg–1AC (as milled)	7.8	85	4.519	3.022	15	4.521	5.438	4.934	0	–	–
Mg–2AC (as milled)	5.5	81	4.519	3.019	17	4.521	5.438	4.934	2	3.21	5.21
Mg–5AC (as milled)	6.2	83	4.519	3.019	13	4.521	5.438	4.934	4	3.213	5.216
Mg–1EG (as milled)	6.7	90	4.519	3.023	10	4.521	5.438	4.934	0	–	–
Mg–2EG (as milled)	7.3	57	4.520	3.018	4	4.521	5.438	4.934	36	3.213	5.216
Mg–1TEG (as milled)	9.5	91	4.519	3.024	9	4.521	5.438	4.934	0	–	–
Mg (re-hydrogenated)	182	78.3	4.5178	3.0210	0	–	–	–	2.1	3.214	5.211
Mg–1AC (re-hydrogenated)	45	81.5	4.5177	3.0213	0	–	–	–	7.1	3.2117	5.218
Mg–5G (re-hydrogenated)	43	86.2	4.5200	3.0223	0	–	–	–	1.1	3.214	5.211
Mg–5MWCNT (re-hydrogenated)	57	83.5	4.5193	3.0217	0	–	–	–	2.1	3.215	5.210
Mg–1EG (re-hydrogenated)	106	90.0	4.5164	3.0205	0	–	–	–	7.4	3.2119	5.213
Mg–2EG (re-hydrogenated)	42	81.5	4.5176	3.0211	0	–	–	–	8.2	3.2138	5.212
Mg–1TEG (re-hydrogenated)	125	94.1	4.5162	3.0201	0	–	–	–	4.9	3.212	5.215

(n = 1, 1.5, 2, and 2.5 for different nucleation mechanisms and growth dimensionalities).

The hydrogenation during the HRBM studied using Fritsch P6 and Retsch PM100 showed a nice agreement between the two experimental sets, with just one exception for Mg–5MWCNT. In the latter case, the incubation period of hydrogenation during the ball milling in Fritsch P6 was about seven times longer than one observed during milling in Retsch PM100, and had approximately the same value as the incubation period for Mg–5G (~2 h) observed for both types of planetary mills. Since the only difference in the ball milling conditions was in the vial dimensions (d = 65 mm × h = 28 mm and d = 75 mm × h = 50 mm for Fritch and Retch, respectively), one may assume them to affect the milling process and to be responsible for the differences in behaviour noticed for Mg–MWCNT during the HRBM. It is reasonable to propose that the bigger vial diameter in case of Retsch ball mill results in higher (~1.15×) linear speeds and centrifugal forces at the same rotation speed, and thus increases the mechanical energy supplied to the charge during the HRBM.

The incubation period is much shorter or absent for other forms of carbon additives in the experiments performed using Retsch PM100 mill (Table 1).

The material with 1 wt.% of MWCNT (Fig. 1A) absorbed hydrogen without an incubation period, but slower than pure Mg; thus, ball milling for 8 h was necessary for reach saturation of the sample with hydrogen. Further increase of the MWCNT content resulted in a significant improvement of the hydrogenation kinetics, which become superior as compared to pure Mg; for Mg–5MWCNT the saturation was achieved in less than 1.5 h of the HRBM (Fig. 1B).

The addition of AC (⩾2 wt.%) also improves the hydrogenation kinetics, but to a lesser extent than that for the Mg–MWCNT materials (Fig. 1B). However, at the lowest content of the AC, 1 wt.% (Fig. 1A), a sharp increase in the hydrogenation rate is observed, similar to the hydrogenation performance of the Mg–5MWCNT.

Hydrogenation of the materials containing EG proceeds slower than that for the pure Mg; the hydrogenation rates slow down with the increase of EG content. As example, for the Mg–2EG sample less than 5 wt.% H is absorbed within a 6 h long HRBM. An increase in EG contents to 5 wt.% resulted in almost complete suppression of H absorption under the stated experimental conditions; the material Mg–5TEG exhibits a similar performance (Fig. 1B). At the same time, the material containing the lowest quantity of EG (1 wt.%) has relatively better hydrogenation performances, which are very close to that observed for Mg–1G. Replacement of the EG with TEG (1 wt.%) resulted in significant improvements of the hydrogenation performances (Fig. 1A).

Observed results agree with the data of [18], where the best hydrogenation performance during the HRBM was observed for the materials containing amorphous carbon and highly-dispersed graphite. However, in our study the hydrogenation was much faster, within 1–5 h, due to use of higher milling energy, application of higher H_2 pressures and adding smaller quantities of carbon additives. Similar origin has a discrepancy of our results with recently published data on HRBM of Mg with 10 wt.% graphite [26].

It should be noted that for some carbon-containing materials, measured hydrogen storage capacities exceeded the values corresponding to the formation of a stoichiometric magnesium dihydride MgH_2. We believe this is caused by a combination of (a) hydrogen chemisorption by the milled nanocarbon; (b) hydrogen trapping in the lattice defects and on the grain boundaries of MgH_2; (c) methanation process. A synergy of the mechanisms (a–c) probably contributes to the outcome of the overall process. Maximum excess capacity, 0.44 wt.% from the total capacity of 8.1 wt.% H, which is observed for Mg–5G, shows that hydrogen–carbon interactions are deeper than the earlier reported in [7–9] for the hydrogenated carbon containing 6–7.5 wt.% H. The difference is probably caused by the more energy intensive milling at higher pressures causing significant contribution from the hydrogen trapping in the defects/at the grain boundaries.

All Mg–C hybrid materials, independent of type and amount of carbon additive, were found to be extremely pyrophoric, especially after completed hydrogen desorption.

3.2. XRD

XRD studies of the materials after HRBM (Table 2) confirmed a completeness of the hydrogenation of Mg to yield MgH_2 for all studied samples, except for Mg–xEG ($x \geqslant 2$ wt.%). Detailed data are given in the Supplementary information, Section S3.

Typical XRD pattern for as-milled Mg and Mg–C are presented in Fig. 2. The samples exhibit broad peaks corresponding to two main constituent phases, a rutile-type α-MgH_2 and a metastable orthorhombic γ-MgH_2 [32]. The experimentally measured content of γ-MgH_2 varies from 4–6% to 18–24%; the upper value is close to the value observed in our earlier work (Denys et al. [27]) in the course of SR XRD study of HRBM Mg (28.5%). The amount of γ-MgH_2 formed in the Mg–C materials has a trend towards its lowering, especially, for C = EG and TEG; the latter samples also showed reduced microstrains in the crystallites of α-MgH_2. The crystallite size of both hydride phases was quite small, 7(1) nm in average. The minimum values, below 6 nm, were observed for Mg–2AC and Mg–5MWCNT. The maximum crystallite size (9.5 nm, 36% higher than the average value) was observed for Mg–1TEG.

The ball milled sample Mg–2EG (Table 2) contained the lowest amount of γ-MgH_2. Its conversion to MgH_2 gave the poorest yield, so a significant amount of unreacted Mg was observed.

Comparison of the SR XRD pasterns of Mg–5MWCNT before the end of the incubation period (Fig. 2C) and after completion of HRBM (Fig. 2D) shows interesting changes. In the former case the pattern contain sharp peaks belonging to the major phase of the unreacted Mg and showing a pronounced texture along (100) direction, together with the peaks of the incipient α-MgH_2 phase whose crystallite size was found to be about three times higher than that for MgH_2 after the HRBM.

No contribution from crystalline carbon-based phases was observed in the XRD pattern that testifies about (a) disappearance of the crystalline graphite-like phases (C = G, EG, TEG), and (b) absence of the chemical interaction between Mg and C yielding magnesium carbide. Moreover, absence of dissolu-

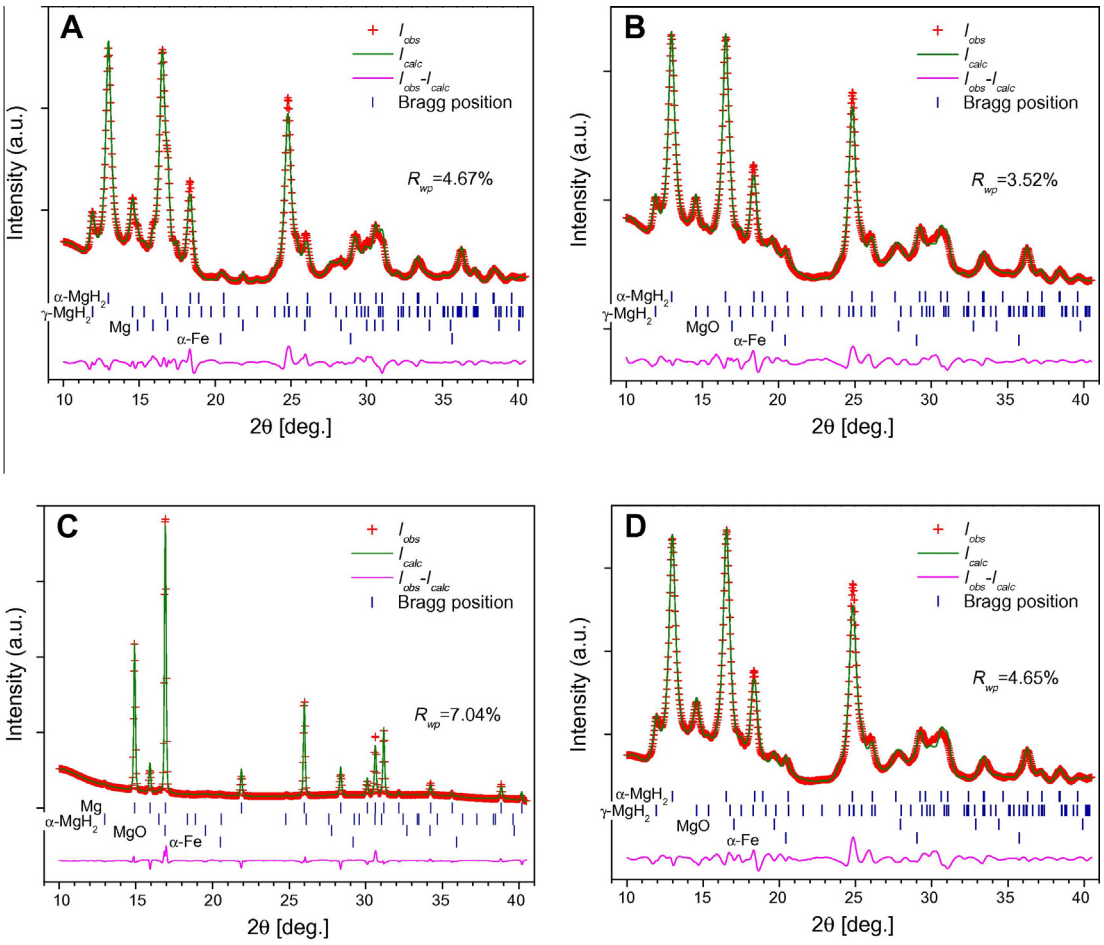

Fig. 2 – SR XRD patterns (SNBL, BM01A; λ = 0.72085 Å) for the as-milled samples of Mg (A), Mg–5G (B) and Mg–5MWCNT collected before the end of the incubation period (C) and after a completion of the HRBM (D).

tion of carbon in Mg and MgH_2 during the HRBM can be confirmed by a very good agreement between the values of their unit cell parameters with the ones specific for HRBM Mg and reported in the reference data (see Table 2).

Most of the C-containing materials also show the presence of MgO presumably formed due to a slight oxidation of Mg/MgH_2 after the HRBM during storage and preparation of the samples for the XRD analysis. In addition, the SR XRD pattern also show the presence of trace amounts of α-Fe (<0.5 wt.% for BPR 40, and ~1 wt.% for BPR 80) contamination from the milling tools.

Patterns of the re-hydrogenated samples (Fig. 3) exhibit sharp peaks corresponding to the well-crystallized α-MgH_2 as a major phase constituent. The unit cell parameters of α-MgH_2 (Table 2) are similar for all studied samples and well agree with the reference data. The pattern also indicates the presence of minor amounts of unhydrogenated Mg (1–8%). Re-hydrogenation resulted in a significant increase in the crystallite size of α-MgH_2 due to its re-crystallisation in the course of the TDS–hydrogenation cycling. However, C-containing hybrid materials show much smaller crystallite size for MgH_2, nearly four times lower than the value for the re-hydrogenated HRBM Mg (Table 2). This was evidenced by differences in the peak broadening of the XRD pattern (see inset in Fig. 3).

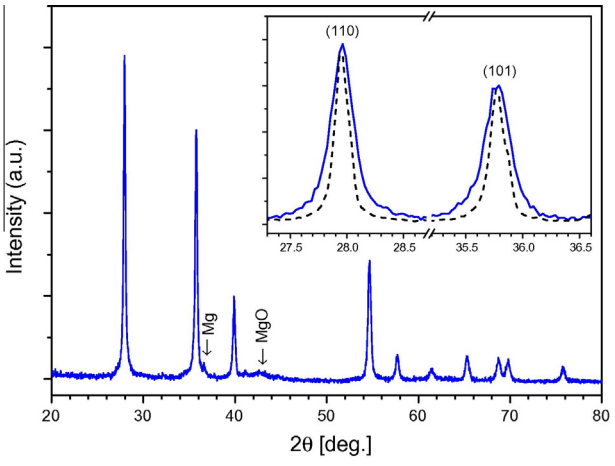

Fig. 3 – XRD pattern of the re-hydrogenated Mg–5G material (Cu-K_α). Inset shows comparison of the peak broadening of α-MgH_2 in re-hydrogenated RBM Mg (dash line) and Mg–5G (solid line).

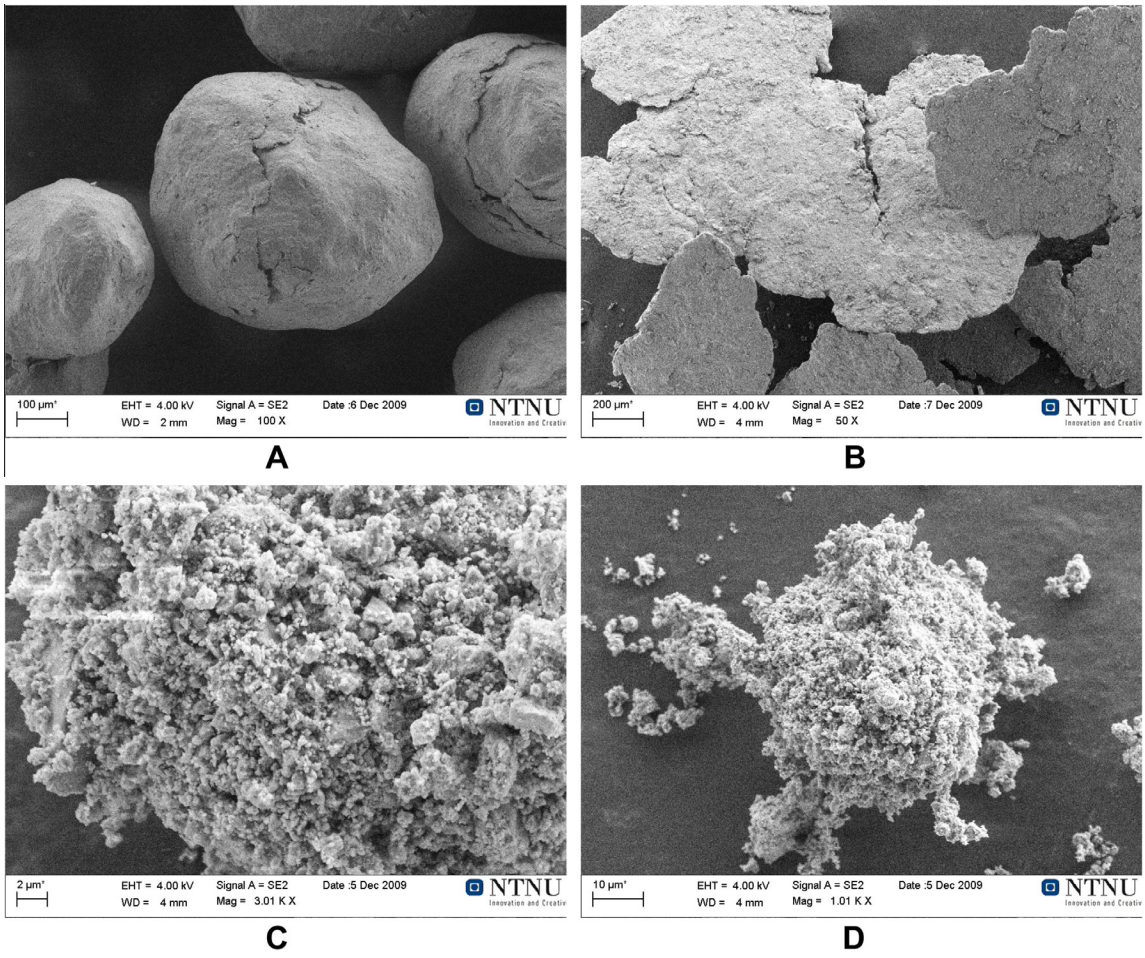

Fig. 4 – SEM images of the studied materials: (A) Mg powder before the HRBM; (B) HRBM Mg–5MWCNT before the end of the incubation period; (C) MgH_2 after 6 h long HRBM of the magnesium; (D) Mg–5MWCNT after completion of the hydrogenation during the HRBM. The Mg–5MWCNT samples (B and D) were characterised by SR XRD (Fig. 2C and D). Scale bars correspond to 100 (A), 200 (B), 2 (C) and 10 (D) µm.

The observed for MgH_2 crystallite sizes in the Mg–C materials (5–7 for as-milled and 40–100 nm for the re-hydrogenated samples; see Table 2) well agree with the values reported by Fuster et al. [17] for Mg–G (5 nm for as-milled and 30–70 nm for the re-hydrogenated samples).

3.3. *Morphology*

The starting magnesium powder consists of particles of regular, close to spherical shape of several hundreds µm in size with smooth surfaces and a very few cracks (see Fig. 4A).

Before the beginning of intense hydrogen absorption, the HRBM material consists of quite large (hundreds µm) plates formed by "forging" of the individual spherical particles of magnesium (Fig. 4B). This morphology is in agreement with the XRD data (Table 2) indicating a significant texture of Mg crystallites. The plates exhibited quite smooth and uniform surfaces, and the carbon material was not discernible in the micrograph indicating that it was homogeneously dispersed on the magnesium particles. Further milling (Fig. 4C and D) resulted in the formation of porous agglomerates of MgH_2.

Measurements of the mean particle sizes of HRBM samples showed that for pure magnesium it is equal to 1.8(1) µm. At the same time, the materials containing G and MWCNT showed a two-fold reduction in size, down to 0.84(9)–0.89(8) µm.

According to the TEM studies, the as-prepared samples contain irregularly shaped grains of various sizes, with larger grains exhibiting a nanoscale twining. Mg and MWCNT were observed to be fully mixed with nanometre size particles of MWCNTs embedded into the MgH_2 aggregates. Twining takes place in the ball-milled MgH_2 [33], and was also observed in the present study in the re-hydrogenated samples (see Supplementary information, Fig. S6C and D). Importantly, the particle sizes of the re-hydrogenated samples are similar to the values for the as-milled materials; these are also in a good agreement with the value of 1.13(9) µm measured for the re-hydrogenated HRBM Mg and Mg–C.

Fig. 5 shows HRTEM images of the re-hydrogenated HRBM Mg (A and B), and Mg–5AC (C and D).

It is clear that carbon additives influence the final dimensions of the ball-milled materials, where smaller particle size is observed with introduction of the additive (compare images

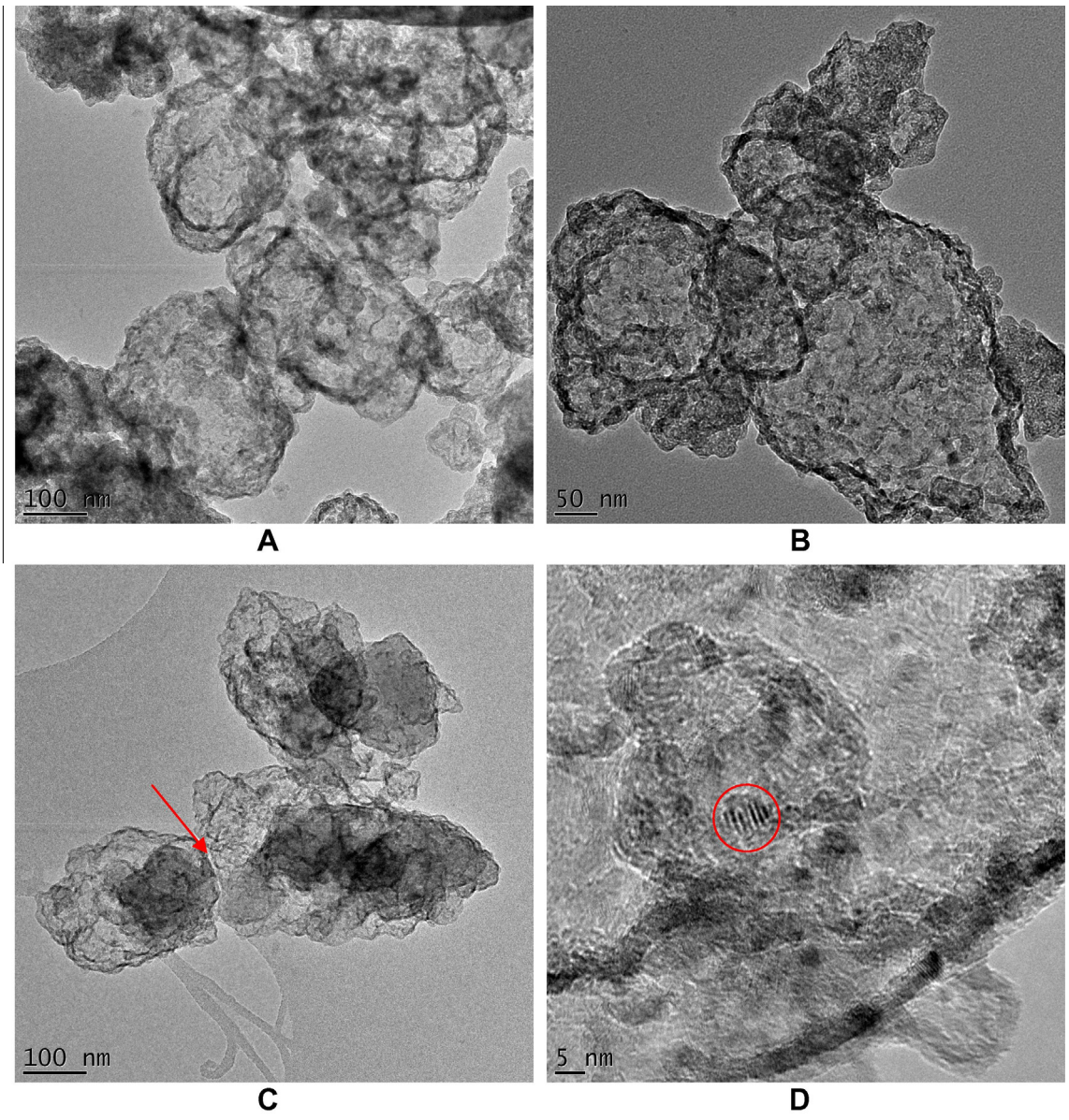

Fig. 5 – TEM images of re-hydrogenated HRBM Mg (A and B), and Mg–5AC (C and D). Scale bars correspond to 100 (A and C), 50 (B), and 5 (D) nm. The arrow shows separation between the neighbouring MgH_2 particles, and circle delimits crystalline area of Mg.

A and C taken at the same magnification). Sintering of the re-hydrogenated MgH_2 particles takes place for pure Mg (Fig. 5A and B) while in the carbon-containing materials a separation between the particles of the hydride (indicated by arrow in Fig. 5C) is clearly observed. The high magnification image (Fig. 5D) shows the presence of few areas belonging to the unhydrogenated magnesium (circled) embedded into the MgH_2 matrix, in agreement well with the XRD results (Table 2). A direct location of the carbon-based species in the hybrid materials was not possible because of (a) deep transformations in carbon during the milling in hydrogen gas which decreased sizes of carbon particles; (b) small content of carbon in the materials; and (c) similar electron transparencies of magnesium and carbon. Thus, we cannot compare our data from the microstructural characterisation and related literature findings based on studies of carbon nanomaterials showing typical morphologies of MWCNT [16]; or studies of the graphitic structure where a good agreement between observed interlayer distances and X-ray diffraction data for the d_{001} spacing takes place [17].

Further details on the morphological studies of the as milled and re-hydrogenated materials are presented in the Supplementary information, see Section S4.

3.4. *De-hydrogenation and re-hydrogenation performances*

Fig. 6 presents typical DSC curves (T = 250–500 °C) for the selected samples. Detailed TGA/DSC data are summarised

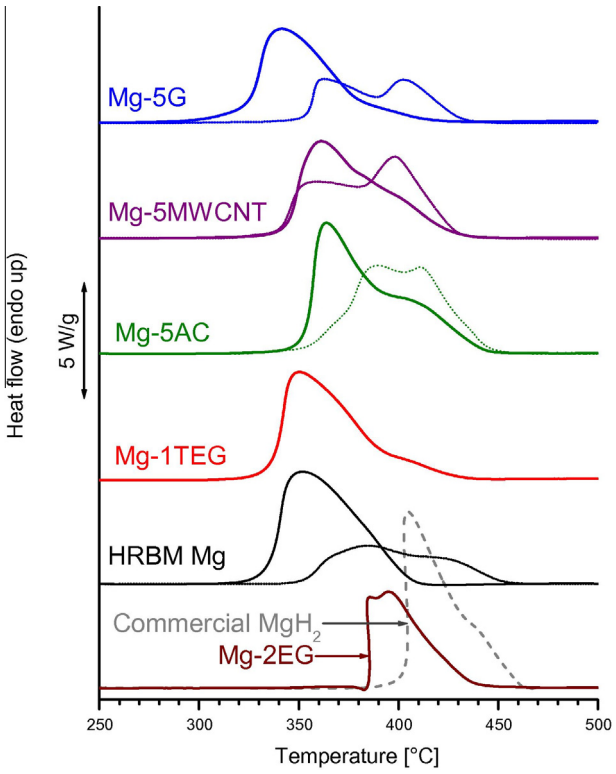

Fig. 6 – Typical DSC curves (heating rate 5 °C/min) for as-milled/as-delivered samples. The curves taken for air-exposed samples are shown as dotted lines.

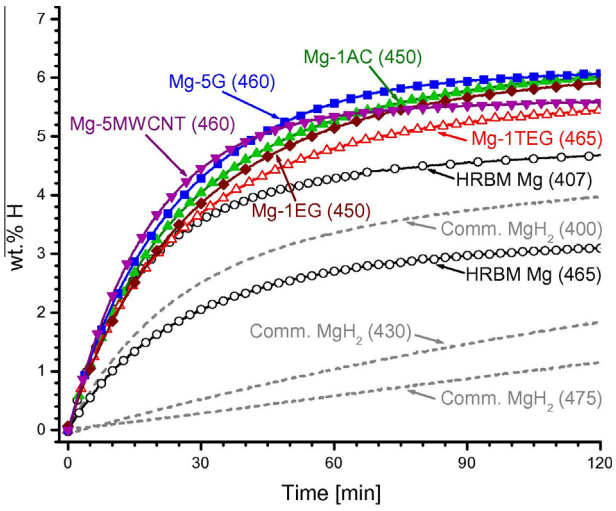

Fig. 7 – Kinetics of re-hydrogenation at 250 °C and 15 bar H_2 of the samples de-hydrogenated by vacuum heating (maximum temperature is specified in brackets).

in Table 3; selected examples of the DSC/TGA and TDS traces are also presented in the Supplementary information (Section S5, Fig. S8). TDS and DSC behaviours were quite similar, with gas evolution peaks for the TDS shifted towards the higher temperatures.

An important feature was a very high sensitivity of the DSC and (for the as-milled samples) TDS traces on the pre-history of the samples. A one-month storage of the samples in a glove box, or several seconds air-exposure of the crucible with the studied sample during its installation in the sample holder, resulted in increase of the decomposition onset and peak temperatures, as well as led to the appearance of the several peaks in the decomposition traces (see corresponding plots in Fig. 6 labelled as "air-exposed", dotted lines). This shows a high affinity of the HRBM Mg–C hybrid materials towards oxidation and is in line with their other observed features, including high pyrophoricity and easy oxidation leading to the observed by the XRD study formation of MgO. The re-hydrogenated samples were found to be more oxidation-sensitive as compared to the as-milled materials, as witnessed by the XRD studies.

In contrast with commercial MgH_2 whose decomposition starts at $T = 390$ °C with a very sharp peak at $T = 404$ °C followed by a gradual decrease of the decomposition rate, the ball milled materials (except of Mg–2EG) were character-

Table 3 – Summary of the DSC/TGA results of the studies of commercial MgH_2, HRBM Mg, and Mg–C hybrid materials.

Sample	Decomposition temperature range (°C)	Peak temperature (°C)	Weight loss (%)	Dehydrogenation heat effect (kJ/mol H_2)
Commercial MgH_2	390–470	404	6.96	78.5
Mg (as milled)	320–415	355	7.15	71.6
Mg (re-hydrogenated)	332–458	365	5.54	76.6
Mg–5G (as milled)	280–430	341	6.97	61.6
Mg–5G (re-hydrogenated)	283–400	347	6.51	73.9
Mg–5MWCNT (as milled)	300–455	361	6.99	65.5
Mg–5MWCNT (re-hydrogenated)	291–413	348	6.62	74.1
Mg–1AC (as milled)	310–435	359	7.30	70.7
Mg–1AC (re-hydrogenated)	295–440	357	6.64	74.2
Mg–5AC (as milled)	315–460	364	7.76	74.8
Mg–5AC (re-hydrogenated)	290–422	360	6.35	73.8
Mg–1EG (as milled)	302–450	351	7.06	70.0
Mg–1EG (re-hydrogenated)	320–455	371	6.27	81.7
Mg–2EG (as milled)	380–470	390	4.66	70.7
Mg–1TEG (as milled)	300–445	351	6.74	73.3
Mg–1TEG (re-hydrogenated)	331–445	382	6.64	79.0

Table 4 – Re-hydrogenation characteristics of magnesium and magnesium–carbon hybrid materials.

Sample[a]	Conditions		Fitted kinetic parameters (Eq. (1))[b]			
	Preceding dehydrogenation temperature (°C)	Cycle #	C_{max} (wt.% H)	t_R (min)	n	Pearson correlation coefficient, R^2
Commercial MgH_2 (7.66)	400	2	4.160(3)	33.70(7)	0.873(1)	0.99918
	430	2	4.981(2)	261(1)	1.003(1)	0.99964
	475	1	4.223(1)	324.2(2)	1.172(1)	0.99934
HRBM Mg (7.66)	407	2	4.976(1)	23.47(5)	0.731(2)	0.99323
	465	1	3.405(1)	35.05(5)	0.726(1)	0.99365
Mg–1G (7.58)	450	1	5.640(2)	29.86(4)	0.882(1)	0.9995
	450	2	5.101(2)	36.42(3)	0.952(1)	0.9999
Mg–5G (7.29)	460	1	6.067(3)	24.32(2)	1.047(1)	0.99988
	460	2	6.145(6)	24.66(3)	0.951(1)	0.99991
Mg–1MWCNT (7.58)	400	1	5.092(2)	24.17(4)	0.843(2)	0.99885
	430	2	5.261(2)	35.78(4)	0.837(1)	0.9993
Mg–2MWCNT (7.51)	430	1	5.585(1)	17.18(5)	0.569(1)	0.97882
	430	2	5.005(1)	20.01(2)	0.755(1)	0.99893
Mg–5MWCNT (7.29)	470	1	5.375(1)	38.80(7)	0.855(2)	0.98711
	460	2	5.441(1)	18.19(1)	1.028(1)	0.99996
Mg–1AC (7.58)	460	1	6.436(3)	31.60(5)	0.808(2)	0.99742
	470	2	5.360(2)	31.18(2)	0.977(1)	0.99986
Mg–2AC (7.51)	430	1	5.402(2)	20.83(3)	0.679(1)	0.99615
	430	2	5.454(1)	27.96(4)	0.691(1)	0.99478
Mg–5AC (7.29)	400	1	4.189(4)	8.16(2)	0.941(2)	0.99935
	430	2	3.878(4)	12.95(2)	0.973(1)	0.99995
	470	1	4.417(5)	37.01(4)	1.096(1)	0.99995
Mg–1EG (7.58)	450	1	6.141(2)	27.43(1)	0.940(1)	0.99998
	465	2	5.679(2)	46.75(3)	0.982(1)	0.99996
Mg–2EG (7.51)	460	1	5.009(5)	31.64(4)	0.934(1)	0.99996
Mg–1TEG (7.58)	465	1	5.258(3)	25.23(2)	0.890(1)	0.99996
	470	2	4.973(1)	30.40(1)	0.932(1)	0.99996

[a] Theoretical hydrogen capacity (assuming 100% formation of MgH_2 and no hydrogenation of carbon) specified in brackets.
[b] Assuming incubation period, $t_0 = 0$.

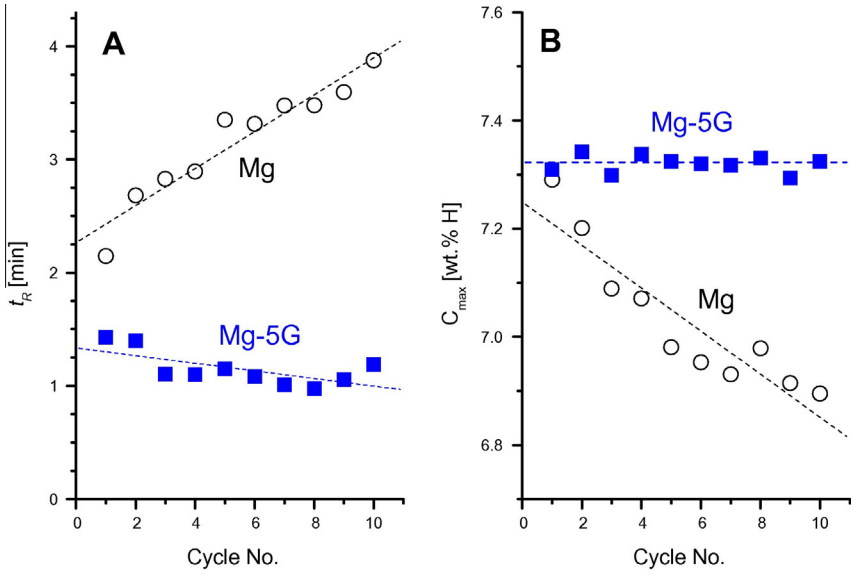

Fig. 8 – Dependencies of characteristic hydrogenation time (inverse to the rate constant) (A) and maximum hydrogen concentration (B) on a number of desorption–absorption cycles at 350 °C for HRBM Mg and Mg–5G hybrid material.

ised by similar de-hydrogenation performances; hydrogen evolution started at $T = 290...320$ °C; it got a peak at $T = 340...380$ °C and was completed at $T = 415...450$ °C.

Estimations of the activation energy of dehydrogenation were performed using the Kissinger method (see Supplementary information, Section S5, Fig. S9) and showed its lowering

for the HRBM Mg and Mg–C hybrid materials, from 188(9) kJ/mol H_2 for the commercial MgH_2, to 95–140 (±3–15) kJ/mol H_2 for the as-milled and re-hydrogenated samples. This is in line with the work by Danaie et al. [28]. At the same time, for the "air-exposed" samples the activation energy increases to 180–220 kJ/mol H_2. In addition, accuracy of the data fitting for the "air-exposed" samples became much lower; corresponding standard deviation increased to 30–50 kJ/mol H_2. However, for the materials containing MWCNT this trend was less pronounced, especially when the amount of the carbon additive increased to 5 wt.%. In addition, the Mg–xMWCNT composites showed noticeable weight increase (up to 0.6 wt.%) at $T > 200$ °C and argon flow of 20 mL/min in the course of TGA/DSC studies. This shows that MWCNT act as a getter of trace amounts of impurities (O_2 and H_2O) which first interact with more reactive carbon atoms forming the end caps. This protects the surface of MgH_2 from interactions with the impurities.

Fig. 7 shows re-hydrogenation performances of the studied samples after *in situ* de-hydrogenation in the course of the TDS studies. The HRBM magnesium and all Mg–carbon hybrid materials exhibited high re-hydrogenation rates, which are superior to that for the de-hydrogenated commercial MgH_2. The amount of hydrogen absorbed in 2.5 h (250 °C/15 bar H_2) varies within 4–6 wt.% H (Table 4).

Kinetics of the re-hydrogenation of the Mg–C hybrid materials was found to be very similar to those for the HRBM Mg indicating that the addition of carbon has minor (if any) catalytic effect. At the same time, maximum H capacity and the re-hydrogenation rate were found to be quite sensitive to the maximum hydrogen desorption temperature applied prior to the re-hydrogenation. The deceleration of the re-hydrogenation takes place with increasing the interaction temperature and is associated with re-crystallisation of Mg resulting in the increase of the grain sizes and corresponding increase of the length of hydrogen diffusion pathways. This effect was found to be much less pronounced for the Mg–C hybrid materials where, according to the XRD data (Table 2), the increase of MgH_2 crystallite size for the re-hydrogenated samples was up to four times smaller than for HRBM Mg without carbon additives. The improvements take place even at low, 1 wt.%, amount of carbon additives, and are particularly pronounced in case of AC, EG and TEG.

Fig. 8 illustrates the effect of carbon on the cycle stability of the HRBM Mg and Mg–C hybrid materials. A clear decrease of both hydrogenation rate and maximum hydrogen absorption capacity was observed for the HRBM Mg. At the same time, addition of carbon to the Mg–C hybrid materials improves their cycle stability. Indeed, the material containing 5 wt.% of graphite shows a stable reversible hydrogen capacity during ten H_2 desorption–absorption cycles, and high rates of the hydrogenation which increase during the first cycles.

3.5. *Discussion*

Present study clearly demonstrates that HRBM of magnesium with carbon additives, even at their minor amount (~1 wt.%) significantly improves hydrogenation–dehydrogenation performance of the Mg–C hybrid materials as compared to magnesium alone.

At the same time, the behaviour of the materials during HRBM strongly depends on the type and amount of the introduced carbon additive. It differently influences the hydrogenation rates during the HRBM (Table 1, Fig. 1), and the temperature variations during the milling. A gradual increase of the vial temperature is less pronounced for the materials containing TEG, EG and G, and has similar and higher rates for Mg alone and for the materials containing AC and MWCNT. It is known [30,31] that ball milling of graphite (both natural and expanded) results in a strong shear effect that results in the delamination process proceeding perpendicular to the *c* direction. It is natural to assume that at the beginning of the HRBM of the materials containing natural, expandable or expanded graphite, part of the mechanical energy is spent to destroy the original graphitic structure and to produce graphene nanosheets.

SEM observations show that prior to the hydrogenation during HRBM, the soft Mg particles are subjected to severe plastic deformation (see Fig. 4A and B). It results in a heating of the material and, finally, the local temperature becomes high enough for the onset of the hydrogenation process. Because the hydrogenation of Mg is rate-limited by a sluggish H diffusion in the formed MgH_2, the absorption process is quite slow and is controlled by the removal of MgH_2 from the surface of the "forged" Mg particles during the ball milling leading to the formation of a "fresh" surface of the unreacted Mg. Graphite as a "soft" carbon material (hardness 0.5–1 Mohs) has a "lubricating" and heat conducting effect thus contributing to (i) improved heat dissipation and thus lowering of the heating rates and (ii) covering of the Mg particles with carbon layers limiting or preventing H_2 supply to the surface of Mg. As a result, no hydrogenation is observed during the incubation period. In contrast, "harder" carbon additives, like AC (hardness $\geqslant$ 3 Mohs), cause "scratching" and milling of Mg particles (hardness 2.5 Mohs) leading to their further disintegration during the HRBM that results in a significant shortening or disappearance of the incubation period. In the case of MWCNT known to be very hard in axial direction and quite soft in radial one, the "scratching" effect becomes pronounced when a sufficient amount of axially-oriented MWCNT will appear, i.e. when the total amount of MWCNT increases.

At the same time, ball milling results in disintegration of the original structure of carbon additives to produce graphene type sheets containing sp^2 hybridized carbon atoms. Indeed, carbon materials studied in present work are built of graphene sheets, which either are rolled into coaxial nanometre-size cylinders (MWCNT), or stacked on the top of each other yielding graphite (G), or graphite-like (TEG, EG) structures. Similarly, AC is formed by curved layers containing pentagons and other non-hexagonal rings in addition to hexagons [34], which can be considered as related to the deformed graphene layers. Graphene layers easily form during the mechanical delamination of graphite [35] and during destruction of the mostly resistant to the milling tubular structures of the MWCNT requiring 2 h of milling at 370–510 rpm [36] to start their fracturing. Note than the latter conditions are quite close to the ones applied in our study, i.e. we operated near the MWCNT fracturing threshold. Thus, depending on the conditions of the experiment (frequency of rotation, milling

time, geometry of the vial and content of MWCNT) we can end up in different stability areas for the MWCNT, where they either remain stable or undergo fracturing during the milling process). This can explain lower reproducibility of the HRBM data obtained using MWCNT, in particular, the differences in the hydrogenation incubation periods obtained using Fritsch P6 and Retsch PM100 ball mills. Delamination of expanded graphite containing graphene planes with increased by ~2% c-interlayer distances, is much easier. The processes of folding and generation of the defects contribute at higher content of EG (which, most probably, exfoliates during the ball milling) and TEG (where ball milling is known to result in folding of the crinkled graphite sheets and in generating in-plane defects [30]).

Absence of crystalline carbon-containing phases in the as milled and rehydrogenated materials was confirmed by Synchrotron XRD studies. Thus, we assume that carbon is present either in amorphous form or, as the stacked graphene layers. The thickness of the latter layers is small, not exceeding ten atomic layers; resulting in absence of the X-ray diffraction pattern. Similar effect of the disappearance of (002) peak was observed in [7,8] during HRBM of the individual graphite.

Carbon is known to act as a lubricating agent during the ball milling of Mg or MgH_2 thus reducing the agglomeration of the particles [14,22]. This result has been confirmed in our study according to which particle size for the as-milled Mg–C materials was two times smaller than the one for HRBM Mg. Furthermore, according to the results of this work, carbon additives inhibit the re-crystallisation processes thus resulting in an increase in the cycle life of the Mg-based hydrogen storage materials. This effect, however, is less pronounced for the re-hydrogenated samples containing small amounts (1 wt.%) of EG and TEG where the crystallite size was in the range 106–125 nm, against ~60 nm for Mg–MWCNT, 40–45 nm for Mg–AC, Mg–G and Mg–2EG, and ~180 nm for Mg without carbon additives.

After the HRBM, all the Mg–C hybrid materials, where C = G, EG, TEG, MWCNT or AC, contain nanostructured magnesium/magnesium hydride with crystallite sizes of 7–10 nm and with hydride nanoparticles separated by graphene layers which play a double role in influencing hydrogen absorption and desorption; (a) they prevent growth of the Mg particles during the high temperature cycling, thus assisting in improving cycle resistance of the materials; (b) they provide an interface for the diffusion of the atomic hydrogen to reach Mg/MgH_2. Thus, when the initial carbon structures disintegrate to produce graphene nanosheets, the Mg–C hybrid materials prepared by HRBM start to show a superior hydrogenation performance even at a minor carbon content of 1 wt.%.[3]

An important feature of the formed during the milling graphene "blocks" is in the presence of a 2D electron system (formed by π electrons) in proximity to their "surface" [37]. Presence of the 2D-distributed negative electron charges creates favourable conditions for the spill-over of monatomic hydrogen carrying an effective positive charge. Such observation has been earlier done during the studies of the hydrogen spill-over effect [38]. A possibility for the improvements of hydrogen sorption performances of the Mg–C materials via an H spill-over mechanism was also pointed out by Wu and Cheng [39].

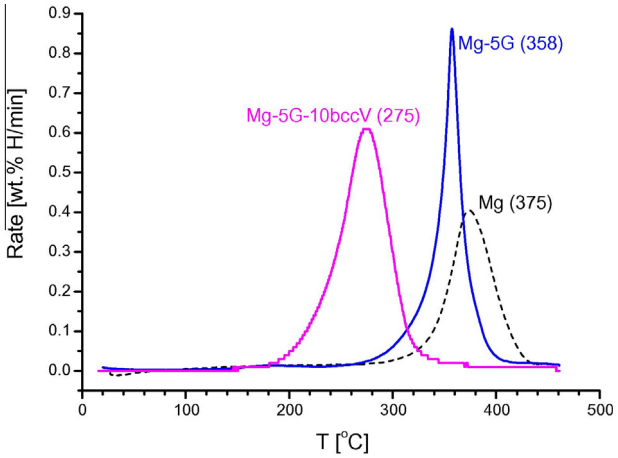

Fig. 9 – TDS curves for the re-hydrogenated HRBM Mg and Mg–5G hybrid materials prepared with and without addition of 10 wt.% of the BCC-V alloy acting as a metal catalyst of hydrogen absorption and desorption. The values of peak temperatures are given in brackets.

Atomic hydrogen is formed by dissociation of hydrogen molecules taking place on the surface of iron nanoparticles produced during the ball milling. The formed hydrogen atoms are further transported via the spill-over mechanism. Thus, carbon plays a role of a carrier of the "activated" hydrogen species while for their formation a presence of a catalyst promoting H_2 dissociation is necessary. The role of iron nanoparticles in the hydrogenation of carbon during the HRBM was discussed in [8]; it was also shown that Fe–C compound formed during the HRBM of carbon by steel milling tools enhances absorption of atomic hydrogen by carbon [9]. Similarly, the metallic catalysts promote recombination of H atoms during dehydrogenation: the improved rates of decomposition of MgH_2 ball milled with CNFs and MWCNTs with metallic impurities (Fe, Ni) were observed by Lillo-Rodenas et al. [16].

Naturally, hybrid materials containing an H_2 dissociation/recombination catalyst in contact with carbon may be characterised by superior hydrogenation/dehydrogenation kinetics.

Indeed, as can be seen in Fig. 9, an addition of 5 wt.% of graphite to magnesium results in lowering of the TDS peak temperature by 17° only (as compared to the re-hydrogenated HRBM Mg), while for the Mg–5G additionally containing 10 wt.% of the catalyst (for example, in a form of a BCC vanadium-based hydride-forming alloy) the peak of hydrogen desorption moves to the lower temperatures by 100°. Significant improvements of the hydrogenation kinetics during the HRBM were also observed: for example, near a complete hydrogenation of Mg–5EG (which does not absorb significant

[3] The threshold of graphene concentration in polymer-based composite materials, where sharp changes in electric conductivity take place, is as low as 0.1 vol.%. [40]. Thus, even minor amount of graphene present in a composite or hybrid material may strongly modify electronic properties and affect the hydrogenation/dehydrogenation performances of Mg–C.

amounts of hydrogen; see Fig. 1B) in presence of the BCC V alloy was reached in just ~1.5 h.

At the same time, graphene has a very high chemical affinity to oxygen, even when oxygen is bound into oxides, e.g. SiO_2 [35] and H_2O [40]. Thus, formation during the milling of the graphene-based layers makes the HRBM Mg–C hybrid materials very sensitive to the surface oxidation, which results in (i) their high pyrophoricity, (ii) formation of MgO, and (iii) significant variation of the hydrogen thermal desorption behaviour after exposure to the gases, containing even trace amounts of oxygen and water vapours.

4. Conclusions

Time-resolved studies of the hydrogenation process have been performed thus allowing to uncover kinetics and mechanism of the Mg–hydrogen interactions in presence of various types of carbon during the High energy ball milling. HRBM of magnesium with minor amounts of additives ($\geqslant$1 wt%) of different carbon materials, including graphite, activated carbon, multi-wall carbon nanotubes, expandable and thermally-expanded graphite, was studied in present work and related to the type and amount of carbon. Structure, morphology, hydrogen absorption and desorption performances of the obtained hybrid materials were characterised using a number of complementary techniques including XRD and synchrotron XRD, particle size measurements, high resolution SEM and TEM, TGA/DSC, TDS, and volumetric measurements of the re-hydrogenation kinetics. Hydrogen absorption data was processed using formal kinetic analysis and yielded kinetic parameters of the (re)hydrogenation processes.

The HRBM of magnesium with carbon materials results in the formation of the Mg–C hybrid materials exhibiting the following properties:

- Complete hydrogenation of magnesium to yield MgH_2 takes place and is accompanied by the formation of materials where carbon is uniformly distributed in between the nanoscale MgH_2 particles.
- Mg–C hybrid materials possess improved hydrogenation kinetics, as compared to a pure Mg. The additives of activated carbon and thermally-expanded graphite induce significant acceleration effect on the hydrogenation process already at their low content of 1 wt.%. For the anisotropically "hard" carbon materials like MWCNT, a larger amount of additive, 5 wt.%, is required to achieve the same increase in the hydrogenation rates.
- Appearance of an incubation period of hydrogenation of magnesium with additive of graphite is observed, which is required to delaminate the graphene layers from the bulk graphite. Similarly, the incubation period also appears for the MWCNT to start their fracturing; the duration of the incubation period is quite sensitive to the ball milling conditions and can be controlled by the optimisation of the vial size and the rotation speed.
- Reduction of MgH_2 particle size in the as-milled Mg–C materials, and lowering of the crystallite size for the MgH_2 formed in the re-hydrogenated samples, as compared to the HRBM Mg.
- Improved hydrogen absorption–desorption cycle life and temperature stability of the hybrid materials tolerating cycling at as high temperature as 460 °C.

The destruction of the carbon species during the HRBM, to form stacked graphene layers, plays a vital role in causing favourable changes and in facilitating the hydrogenation kinetics because of the formation of hydrogen-transferring interfaces on the phase boundaries between the carbon and the formed MgH_2.

Analysis of the experimental data shows absence of the direct catalytic effect of carbon on hydrogenation–dehydrogenation of Mg and suggests that carbon plays a role of a carrier of the "activated" hydrogen by the spill-over mechanism.

Dehydrogenation performances of the magnesium–carbon hybrid materials were found to be very sensitive to the exposure to the gases containing even trace amounts of oxygen and water vapours. The "air-exposed" samples are characterised by higher dehydrogenation temperatures and appearance of a multipeak hydrogen desorption behaviour. The "air-exposure" effect becomes however less pronounced for the materials containing multi wall carbon nanotubes.

Acknowledgements

This work was supported by Hydrogen and Fuel Cell Technologies RDI Programme (HySA), funded by the Department of Science and Technology (DST) in South Africa (Project KP3-S04); as well as by the Program of Research Co-operation between Norway and South Africa (2007–2010, Project #180344). The support of the National Research Foundation (NRF) of South Africa via Incentive Funding Grants (ML) is acknowledged as well.

Appendix A. Supplementary data

Supplementary data associated with this article can be found, in the online version, at http://dx.doi.org/10.1016/j.carbon.2013.01.058.

REFERENCES

[1] Jain IP, Lal C, Jain A. Hydrogen storage in Mg: a most promising material. Int. J. Hydrogen Energy 2010;35:5133–44.
[2] Konstanchuk IG, Ivanov E, Pezat M, Darriet B, Boldyrev VV, Hagenmuller P. The hydriding properties of a mechanical alloy with composition Mg–25%Fe. J Less-Common Met 1987;131:181–9.
[3] Zaluska A, Zaluski L, Ström-Olsen JO. Nanocrystalline magnesium for hydrogen storage. J Alloys Compds 1999;288:217–25.
[4] Bobet JL, Chevalier B, Song MY, Darriet B, Etourneau J. Hydrogen sorption of Mg-based mixtures elaborated by reactive mechanical grinding. J Alloys Compds 2002;336:292–6.
[5] Lototsky MV, Denys RV, Yartys VA. Combustion-type hydrogenation of nanostructured Mg-based composites for hydrogen storage. Int J Energy Research 2009;33:1114–25.

[6] Imamura H, Kusuhara M, Minami S, Matsumoto M, Masanari K, Sakata Y, et al. Carbon nanocomposites synthesized by high-energy mechanical milling of graphite and magnesium for hydrogen storage. Acta Mater 2003;51:6407–14.

[7] Orimo S, Majer G, Fukunaga T, Züttel A, Schlapbach L, Fujii H. Hydrogen in the mechanically prepared nanostructured graphite. Appl Phys Lett 1999;75:3093–5.

[8] Smith CI, Miyaoka H, Ichikawa T, Jones MO, Harmer J, Ishida W, et al. Electron spin resonance investigation of hydrogen absorption in ball-milled graphite. J Phys Chem C 2009;113:5409–16.

[9] Miyaoka H, Ichikawa T, Fujii T, Ishida W, Isobe S, Fuji H, et al. Anomalous hydrogen absorption on non-stoichiometric iron–carbon compound. J Alloys Compds 2010;507:547–50.

[10] Huot J, Tremblay ML, Schulz R. Synthesis of nanocrystalline hydrogen storage materials. J Alloys Compds 2003;356–357:603–7.

[11] Shang CX, Guo ZX. Effect of carbon on hydrogen desorption and absorption of mechanically milled MgH_2. J Power Sources 2004;129:73–80.

[12] Chen D, Chen L, Liu S, Ma CX, Chen DM, Wang LB. Microstructure and hydrogen storage property of Mg/MWNTs composites. J Alloys Compds 2004;372:231–7.

[13] Wu CZ, Wang P, Yao X, Liu C, Chen DM, Lu GQ, et al. Effect of carbon/noncarbon addition on hydrogen storage behaviors of magnesium hydride. J Alloys Compds 2006;414:259–64.

[14] Huang ZG, Guo ZP, Calka A, Wexler D, Liu HK. Effects of carbon black, graphite and carbon nanotube additives on hydrogen storage properties of magnesium. J Alloys Compds 2007;427:94–100.

[15] Lukashev RV, Tarasov BP, Klyamkin SN. MgH_2–carbon composites for hydrogen storage. In: Veziroglu TN et al. (editors). NATO security through science series A: chemistry and biology; 2007. pp. 193–97.

[16] Lillo-Rodenas MA, Guo ZX, Aguey-Zinsou KF, Cazorla-Amoros D, Linares-Solano A. Effects of different carbon materials on MgH_2 decomposition. Carbon 2008;46:126–37.

[17] Fuster V, Castro FJ, Troiani H, Urretavizcaya G. Characterization of graphite catalytic effect in reactively ball-milled MgH_2–C and Mg–C composites. Int J Hydrogen Energy 2011;36:9051–61.

[18] Rud AD, Lakhnik AM. Effect of carbon allotropes on the structure and hydrogen sorption during reactive ball-milling of Mg–C powder mixtures. Int J Hydrogen Energy 2012;37:4179–87.

[19] Jia Y, Guo Y, Zou J, Yao X. Hydrogenation/dehydrogenation in MgH_2-activated carbon composites prepared by ball milling. Int J Hydrogen Energy 2012;37:7579–85.

[20] Spassov T, Zlatanova Z, Spassova M, Todorova S. Hydrogen sorption properties of ball-milled Mg–C nanocomposites. Int J Hydrogen Energy 2010;35:10396–403.

[21] Skripnyuk VM, Rabkin E, Bendersky LA, Magrez A, Carreño-Morelli E, Estrin Y. Hydrogen storage properties of as-synthesized and severely deformed magnesium – multiwall carbon nanotubes composite. Int J Hydrogen Energy 2010;35:5471–8.

[22] Aminorroaya S, Liu HK, Cho Y, Dahle A. Microstructure and activation characteristics of Mg–Ni alloy modified by multi-walled carbon nanotubes. Int J Hydrogen Energy 2010;35:4144–53.

[23] Pohlmann C, Röntzsch L, Kalinichenka S, Hutsch T, Kieback B. Magnesium alloy-graphite composites with tailored heat conduction properties for hydrogen storage applications. Int J Hydrogen Energy 2010;35:12829–36.

[24] Delhomme B, de Rango P, Marty P, Bacia M, Zawilski B, Raufast C, et al. Large scale magnesium hydride tank coupled with an external heat source. Int J Hydrogen Energy 2012;37:9103–11.

[25] Doppiu S, Schultz L, Gutfleisch O. In situ pressure and temperature monitoring during the conversion of Mg into MgH_2 by high-pressure reactive ball milling. J Alloys Compds 2007;427:204–8.

[26] Castro FJ, Fuster V, Urretavizcaya G. MgH_2 synthesis during reactive mechanical alloying studied by in situ pressure monitoring. Int J Hydrogen Energy 2012;37:16844–51.

[27] Denys RV, Riabov AB, Maehlen JP, Lototsky MV, Solberg JK, Yartys VA. In situ synchrotron X-ray diffraction studies of hydrogen desorption and absorption properties of Mg and Mg–Mm–Ni after reactive ball milling in hydrogen. Acta Mater 2009;57:3989–4000.

[28] Danaie M, Tao SX, Kalisvaart P, Mitlin D. Analysis of deformation twins and the partially dehydrogenated microstructure in nanocrystalline magnesium hydride (MgH_2) powder. Acta Mater 2010;58:3162–72.

[29] Karty A, Grunzweig-Genossar J, Rudman PS. Hydriding and dehydriding kinetics of Mg in a Mg/Mg_2Cu eutectic alloy: Pressure sweep method. J Appl Phys 1979;50:7200–9.

[30] Yue X, Wang H, Wang S, Zhang F, Zhang R. In-plane defects produced by ball-milling of expanded graphite. J Alloys Compds 2010;505:286–90.

[31] Duan W. Nanostructure evolution of expanded graphite during high-energy ball-milling. Appl Mech Mater 2011;80–81:229–32.

[32] Bastide JP, Bonnetot B, Létoffé JM, Claudy P. Polymorphisme de l'hydrure de magnésium sous haute pression. Mater Res Bull 1980;15:1215–24.

[33] Danaie M, Mitlin D. TEM analysis and sorption properties of high-energy milled MgH_2 powders. J Alloys Compds 2009;476:590–8.

[34] Harris PJF, Liu Z, Suenaga K. Imaging the atomic structure of activated carbon. J Phys Condens Matter 2008;20:362201.

[35] Novoselov KS, Geim AK, Morozov SV, Jiang D, Zhang Y, Dubonos SV, et al. Electric field effect in atomically thin carbon films. Science 2004;306:666–9.

[36] Tucho WM, Mauroy H, Walmsley JC, Deledda S, Holmestada R, Hauback BC. The effects of ball milling intensity on morphology of multiwall carbon nanotubes. Scr Mater 2010;63:637–40.

[37] Avouris P, Dimitrakopoulos C. Graphene: synthesis and applications. Materials Today 2012;15(3):86–97.

[38] Lobashina NE, Savvin NN, Myasnikov IA. Investigation of the mechanism of hydrogen spillover on deposited metal catalysts III. Nature of the migrating particles. Kinet Catal 1984;25:420–2.

[39] Wu C, Cheng HM. Effect of carbon on hydrogen storage performances of hydrides. J Mater Chem 2010;20:5390–400.

[40] Stankovich S, Dikin DA, Dommett GHB, Kohlhaas KM, Zimmey EJ, Stach EA, et al. Graphene-based composite materials. Nature 2006;442:282–6.